IBRO Neuroscience Reports 12 (2022) 170–181

Contents lists available at ScienceDirect

IBRO Neuroscience Reports

journal homepage: www.sciencedirect.com/journal/IBRO-Neuroscience-Reports

Research paper

Functional connectivity of intercalated nucleus with medial amygdala: A circuit relevant for chemosignal processing

Lindsey M. Biggs [1], Michael Meredith [*]

Program in Neuroscience and Dept. Biological Science, Florida State University, Tallahassee, FL 32306, USA

ARTICLE INFO

Keywords:
Whole-cell slice-recording
Electrical stimulation
Dopamine
GABA
Glutamate
Male Hamster

ABSTRACT

Medial amygdala processes social/reproductive chemosensory input, and its projections to preoptic and hypothalamic areas evoke appropriate behavioral and physiological responses. We and others have shown that different chemosensory signals elicit differential responses in medial amygdala subregions and in adjacent main intercalated nucleus (mICN). The largely GABAergic mICN receives no direct chemosensory input but, as we show, mICN has functional circuit connections with medial amygdala that could be responsible both for mICN chemosensitivity and for a feedforward inhibitory effect on posterior medial amygdala; which, in turn would affect chemosignal response. mICN is subject to inhibition by dopamine and is probably regulated by neuropeptides and input from frontal cortex. Thus, mICN is in position to modify chemosensory processing in medial amygdala and behavioral responses to social signals, according to internal brain state. Patch-clamp recordings from neurons in each relevant nucleus in horizontal brain-slices, with electrical stimulation in adjacent nuclei, reveal multiple functional connections between medial amygdala subregions and mICN. We highlight a triangular circuit which may underlie mICN chemosensitivity and its potential for modifying chemosensory information transmitted to basal forebrain. Anterior medial amygdala, which receives most of the chemosensory input, connects to posterior medial amygdala directly and both areas send information on to basal forebrain. Anterior medial amygdala can also modulate posterior medial amygdala indirectly via the mICN side-loop, which also provides a pathway for modulation by cortical input or, when inhibited by dopamine, could allow a more automatic response – as proposed for other amygdala circuits with similar ICN side loops.

1. Introduction

The amygdala forms a nexus for emotional/motivational assessment of external signals conveyed by most sensory systems (Adolphs, 2010; Lin et al., 2020; Zald, 2003). In most mammals, including rodents, the medial amygdala is a primary processing center for social chemosensory information (Carvalho et al., 2015; Maras and Petrulis, 2010a; Meredith and Westberry, 2004; Newman, 1999; Samuelsen and Meredith, 2009). Here we investigate whether GABAergic neurons of the amygdaloid intercalated nuclei (ICN) could be involved in these chemosensory processing circuits; as they appear to be for other amygdala circuits. We find that caudal main intercalated nucleus (mICNc) has circuit connections with medial amygdala, which can be modulated by dopamine. These relationships are similar to those of other ICN cell-groups with basolateral amygdala, which can modulate pain and anxiety, fear conditioning and extinction (Asede et al., 2015; Duvarci and Pare, 2014; Thompson and Neugebauer, 2017).

Medial amygdala receives chemosensory input from the vomeronasal organ and main olfactory epithelium via the accessory and main olfactory bulbs (Bergan et al., 2014; Cádiz-Moretti et al., 2016; Kang et al., 2009, 2011a, 2011b; Lehman and Winans, 1982; Sosulski et al., 2011; Thompson et al., 2012). Both pathways respond to social signals or information about predators (i.e., semiochemical stimuli), which may be unlearned (Demir et al., 2020; Root et al., 2014). Medial amygdala is critical for normal social/reproductive behaviors in many species (Kondo and Arai, 1995; Maras and Petrulis, 2006, 2010a; Wang et al., 2013; Wood and Coolen, 1997). In rodents, anterior medial amygdala (MeA dorsal and ventral; MeAd/v) receives most of the direct vomeronasal and main olfactory input. MeA relays information to posterior medial amygdala (MeP; dorsal and ventral; MePd/v) and both MeA and MeP have projections to basal forebrain regions, including preoptic area and hypothalamus, which are essential for normal reproductive and social behavior (Been and Petrulis, 2011; Carvalho et al., 2020; Coolen

* Correspondence to: Dept. Biological Science Florida State University, Tallahassee, FL 32306, USA.
E-mail addresses: lbiggs@neuro.fsu.edu (L.M. Biggs), mmeredith@fsu.edu (M. Meredith).
[1] Current address: Dept. Psychology, Florida State University, Tallahassee FL 32306.

https://doi.org/10.1016/j.ibneur.2022.01.005
Received 1 November 2021; Received in revised form 8 January 2022; Accepted 19 January 2022
Available online 2 February 2022

and Wood, 1998; Keshavarzi et al., 2014; Kondo and Arai, 1995; Wang et al., 2013). Amygdala processing is subject to modulation by dopamine (Gregoriou et al., 2019; Marowsky et al., 2005), which can act via GABA input from the intercalated nuclei. It is also influenced by hormones (Been and Petrulis, 2011; Maras and Petrulis, 2006, 2010b, 2010c, 2010a; Wood and Coolen, 1997), including via its aromatase-expressing neurons (Billing et al., 2020); and by neuromodulators (Gregoriou et al., 2019; Samuelsen and Meredith, 2011; Winters et al., 2017; Yao et al., 2017), some of which might also act via ICN.

We have evidence for a modulation of medial amygdala activity by mICNc during chemosensory investigation (Biggs and Meredith, 2020; Meredith and Westberry, 2004). When male hamsters investigate social-signal-odors of (unfamiliar) male or female hamsters (conspecifics), both MeA and MeP are activated (increased immediate early gene (IEG) expression), including GABA-Receptor-ir cells (Westberry and Meredith, 2016). When social signals serving a similar purpose for other (heterospecific) species (male/female mouse urine, cat urine) are investigated by hamsters, MeA is again activated but activity in MeP is non-significant and GABA-R-ir cells are suppressed, suggesting a possible GABAergic inhibition, analogous to that seen in fear circuits. Patterns of activation are different for male and female conspecific signals and again different for heterospecific signals. By altering these patterns, mICNc can play a role both in reduction of onward transmission for heterospecific signals and a modification of the transmitted activity for male vs female conspecific signals.

The anatomical connections within and between medial amygdala and ICN are not well described but our immediate-early gene evidence in hamsters (above) suggests a triangular circuit involving MeA, MeP and mICNc. Here, using in-vitro patch-clamp electrophysiology in a novel brain slice from hamster, we provide evidence for functional connections between the three players in the proposed circuit. We know chemosensory input from main and accessory olfactory bulbs to MeA is relayed to MeP for additional processing (Maras and Petrulis, 2010b). We propose that this process is subject to modulation via a parallel circuit from MeA to MeP via mICNc with excitation from MeA to mICNc followed by feedforward inhibition to MeP. This additional circuit would be differentially activated dependent on the pattern of input to MeA, from male or female conspecific, or heterospecific chemosensory signals received. ICN cell-groups are known to be subject to modulatory input (from DA, neuropeptides and from prefrontal cortex), so this circuit can provide modulation to medial amygdala reflecting brain-state and/or non-chemosensory input. This modulation of the ICN contribution to the chemosignal information entering the basal forebrain provides for additional regulation of behavioral and physiological responses.

2. Methods

All experiments described here were approved by the Florida State University Institutional Animal Care and Use Committee (IACUC) and conducted according to American Veterinary Medical Association and National Institute of Health guidelines. Hamsters were purchased from Charles River Laboratories or bred in house from Charles River stock. They were housed under a reversed 14 h/10 h light/dark cycle such that experimental animals were in the dark cycle when removed for experiments. Adult hamsters were single-housed and dams remained with their litters until the pups were weaned at postnatal day 28. *Ad libitum* food and water was provided. Because our data implicating the proposed circuit in social chemosensory responses of the medial amygdala are from males (Biggs and Meredith, 2020; Meredith and Westberry, 2004; Westberry and Meredith, 2016), we used only males in this study of the circuit connections.

2.1. Acute slice preparation

Male hamsters (*Mesocrocetus auruatus,* postnatal day 14–28) were deeply anesthetized with Isoflurane and decapitated. Neural tissue was quickly removed in ice-cold, oxygenated cutting solution containing (in mM): NaCl 83; $NaHCO_3$ 26.2; NaH_2PO_4 1; $MgCl_2$ 33; $CaCl_2$ 0.5; glucose 22; sucrose 72; pH 7.3–7.4). Brain slices (350 μm thick) were obtained with a Series 1000 Vibratome either in the coronal plane cut perpendicular to the ventral surface of the brain as shown in the Morin and Wood (2001) atlas, (0.2 mm anterior to 0.5 mm posterior to bregma at the level of MeP), or in the horizontal plane parallel to the ventral surface of the brain and approximately 900–1700 μm from the ventral surface. Recordings were made in coronal slices containing MePd and mICNc and in horizontal slices containing MeAd, MePd and mICNc. Slices were incubated in oxygenated artificial cerebrospinal fluid (aCSF: in mM: NaCl 119; $NaHCO_3$ 26.2; KCl 2.5; $CaCl_2$ 2.5; NaH_2PO4 1; $MgCl_2$ 1.3; glucose 22; pH 7.3–7.4) at approximately 33° C for 30–45 min for recovery, then maintained at room temperature with continuous oxygenation until use.

2.2. Whole-cell slice electrophysiology

During electrophysiological recordings, slices were continuously perfused with fresh, oxygenated aCSF, with or without added drugs. Experiments focused on the dorsal regions of the medial amygdala since this area could be contained in the same horizontal slice as the mICNc. Medial amygdala was identified in unstained live tissue slices using anatomical markers including the optic tract and intermediate capsule. The mICNc was identified by the close lateral proximity to the medial amygdala, the small cell size and dense clustering of neurons and by comparison with fixed tissue sections of the same orientation and anatomical level stained for calbindin, where mICNc is an unstained island outlined by stained cells in surrounding regions. Fig. 1 shows horizontal slices as described here, with calbindin and/or calretinin immunoreactive (ir) cells stained and mounted in DAPI-mounting medium which stains cell nuclei. The immunohistochemical methods used are described in detail in Biggs and Meredith (2020). Briefly, animals were deeply anesthetized, perfused with PBS and 4% paraformaldehyde. Horizotal slices were cut at 40uM and incubated (48 hr) with mouse anti-calbindin D-28k (1:10,000; #300, Swant Antibodies) and goat anti-calretinin (1:2500; CG1, Swant Antibodies). Secondary incubation (4 hrs, 4° C) was with donkey anti-mouse Alexa-Fluor 488 (1:500, A-21202, Invitrogen Molecular Probes) for CB immunostaining and/or donkey anti-goat Alexa-Fluor 555 (1:500, A-31572, Invitrogen Molecular Probes) for CR immunostaining. Tissue was then mounted and coverslipped with Vectasheild Hard Set with DAPI (H-1200, Vector Labs) for DAPI visualization.

For electrophysiology, visually identified cells in living 350 μm slices were patched via somatic whole-cell patch clamp using glass borosilicate capillaries (1B150F-3, World Precision Instruments) filled with intracellular solution (in mM: 145 $KMeSO_3$, 1 $MgCl_2$-6 H2O, 10 Hepes, 2 Na-ATP, 0.4 Na-GTP, 1.1 EGTA; pH 7.3–7.4; ~ 280 mOsm). Pipettes were pulled on the Flaming/Brown micropipette puller (P-97, Sutter Instruments) and had an initial resistance between 3 and 8 mOhms depending on the type of neuron; i.e. mICNc cell recordings required a higher resistance pipette due to the small cell size. Whole-cell recording was performed after making a gigaohm seal and only cells with an initial access resistance lower than 30 mOhm indicated by the "Seal/Membrane test" in the pClamp software were accepted for analysis. The series resistance was monitored at random intervals during recording. Cells with large changes in series resistance (>30%), or which appeared unstable were excluded from the analysis. Generally, each cell came from a different slice as slices were always discarded after being exposed to any drugs other than aCSF. Occasionally records from 2 (rarely 3) cells in the same slice were accepted if the slice had been exposed only to aCSF. The number of animals contributing cells to the analysis is given for each figure here. Electrophysiological signals were amplified (Multiclamp 700B, Molecular Devices), low pass filtered (10 KHz) and digitized using the Digidata 1322 A (Molecular Devices) at 2–10 khz. All data were

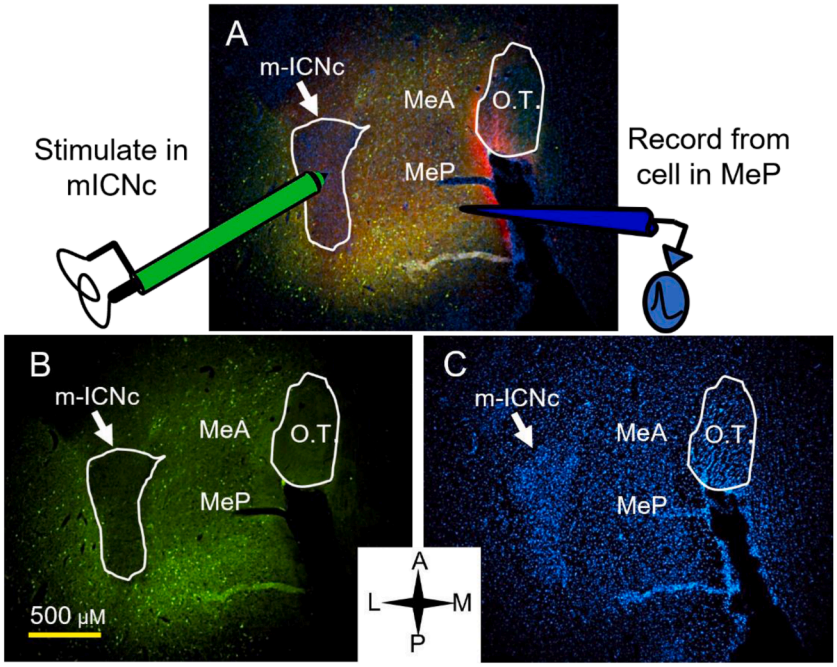

Fig. 1. Layout of horizontal slices through hamster left medial amygdala (anterior up). A) Superimposed immunohistochemistry images for DAPI (blue; showing cell nuclei), calretinin-ir (red) and calbindin-ir (green). Individual images are in B (calbindin-ir) and C (DAPI). Medial amygdala lies lateral (left) to the optic tract (OT) that rises obliquely through the plane of the slice. The accessory olfactory tract enters medially into MeA/P and carries some calretinin-ir fibers. The mICNc appears as a region of dense small cells (in C) that does not stain for calbindin (B; It also contains few if any calretinin-ir cells, A). The intermediate capsule passes obliquely down through the plane of the slice between mICNc and MeA/P. These images were produced using methods detailed in a previous publication: Biggs LM, Meredith M. 2020. "*Activation of Calcium Binding Protein-ir Neurons in Medial Amygdala during Chemosignal Processing. Chem Senses 45 (6):439–448*", which contains additional images. Superimposed on A are cartoons of a bipolar stimulating electrode (left, green) and a whole-cell recording electrode (right, blue) in approximate positions for stimulation of mICNc with recording of cells in MeP. (For interpretation of the references to colour in this figure, the reader is referred to the web version of this article.)

collected using the PClamp software (Version 10, Molecular Devices) and analyzed using Clampfit (Version 10.3, Molecular Devices). The experimentally determined junction potential (−11 mV) was applied to all recordings. As is usual for slice recordings, experiments were conducted at room temperature (~20° C).

For field-stimulation in the various amygdala nuclei, a bipolar stimulating electrode (F. Haer Co. CBFPG75) was used. Monophasic square pulses (500 μs, negative center pole) were controlled through the pClamp software and delivered via a WPI stimulus isolator (A365) so that stimulus current was isolated from the tissue ground and the recording circuit. For each neuron, stimulation was set to the lowest intensity at which an evoked post-synaptic potential (ePSP) was evident (10–30 μA, mean 17.1 μA) to characterize the PSP response. Generally, 10 sweeps were averaged creating one average trace to represent the neuron's response. Where stimulation did elicit action potential firing, those traces were not included in the ePSP analysis. The stimulating electrode was placed in one of several different locations of the anterior or posterior medial amygdala or in mICNc while avoiding fiber bundles of the accessory olfactory tract, laterally and stria terminalis, caudally. ePSPs were recorded in neurons in the other areas to reveal possible functional connections.

Drugs were dissolved in aCSF and bath applied, including various receptor antagonists: picrotoxin (100 μM, P1675–1 G, Sigma-Aldrich), kynurenic acid (3 mM, K3375, Sigma-Aldrich), 6,7 dinitroquinoxaline (DNQX,5 μM, #189, Tocris Bioscience), (2 R)-amino-5-phosphonovaleric acid (APV,10 μM, #106, Tocris Bioscience). For dopamine (DA) experiments, dopamine-HCl (30 μM, H8502, Sigma-Aldrich) and the DAD1 receptor agonist, dihydrexidine (DHX, 2 μM, Tocris Bioscience SCH23390) were used in aCSF with or without receptor blocking drugs in the concentrations given above.

For pharmacological stimulation of mICNc, a glass micropipette (~3 mOhm resistance) containing L-glutamic acid (10 mM in aCSF, G8415 Sigma-Aldrch) was placed superficially into mICNc and a picospritzer (Picospritzer III, Parker) delivered a short puff of L-glutamic acid to the tissue (3.5 psi, 300–500 ms) using a special low-pressure regulator. Spread of ejected fluid to surrounding subnuclei was checked visually in preliminary experiments using a concentrated solution of green food dye. Picspritzer pressure and pulse duration were adjusted to provide reliable depolarization of mICNc neurons without direct action on MePd and with no observable mechanical disturbance. In these experiments, the inhibitory action of mICNc on MePd was characterized by the number of inhibitory post synaptic currents (IPSCs) elicited in voltage clamped MePd neurons for 6 s after the start of mICNc cell stimulation, averaged across 5 sweeps; and compared to a 6 second control period when the Picospritzer was activated but no glutamate was delivered. For IPSC quantification, the baseline was adjusted to a steady level and quantified using the Clampfit Event Detection software. Event detection threshold was set for each cell at greater than 2 x root-mean-square value for the first 400 ms of each sweep with a noise rejection of 5 ms. IPSCs were characterized by a steep rising phase and slower falling phase, substantially above ongoing noise for more than 5 ms, as visually confirmed by an experimenter.

2.3. Statistics

Analyses were performed in Graphpad Prism (V9.2). Paired t-tests and repeated measures one-way ANOVA were performed depending on the type of data set. Paired t-tests were used when a baseline value was being compared to a value collected from the same cell during a drug or angonist/antagonist treatment. In the event that the same cell was exposed to three different bath applications, i.e. baseline, dopamine and washout baths, a one-way RM ANOVA was used. Significant one-way RM ANOVA tests were followed by Tukey post-hoc tests to compare groups. Statistical analyses used for each experiment are indicated in the text.

3. Results

Our principal hypothesis holds that chemosensory information affecting social behavior is processed in part via a triangular circuit from anterior (MeA) to posterior medial amygdala (MeP) directly and via a parallel loop from MeA to MeP via the adjacent GABAergic intercalated nucleus (mICNc). This circuit can be further regulated by dopamine acting via mICNc; as previously proposed for the triangular circuit module involving basolateral and central amygdala with a different cell group of the intercalated nuclei (Duvarci and Pare, 2014). The work presented here demonstrates the necessary connections underlying our proposed triangular circuit involving medial amygdala, and reveals

other connections that could provide additional modulation; all of which could refine information passing from the medial amygdala to the basal forebrain and affect social behavioral responses to chemosensory signals. Fig. 1 illustrates the relationship of MeA, MeP and mICNc with their surrounding landmarks in fixed tissue sections cut in the same horizontal plane as used here.

3.1. The triangular circuit with intercalated nucleus loop

Fig. 2 shows examples of depolarizing (C; putatatively excitatory) and hyperpolarizing (D; inhibitory) responses of MePd neurons to MeAd stimulation in slices perfused with aCSF. A chart of relative ocurrence of different responses in various bath solutions is shown in Fig. 2B. MeAd stimulation had an effect on all recorded MePd neurons (16/16) in aCSF. The majority (62.5%) exhibited a depolarizing excitatory post-synaptic potential (EPSP) followed, in all but one, by an inhibitory post-synaptic potential (IPSP; example in C), suggesting multiple inputs (mono- or poly-synaptic) from MeAd onto many individual MePd neurons. The remaining 37.5% of neurons showed an IPSP only (example in D).

Blockade of the GABAa receptors via picrotoxin (100 μM in aCSF) abolished MeAd induced IPSPs and all neurons in this bath ($n = 8$) showed an MeAd-evoked EPSP (Fig. 2B). For most cells in this group the EPSP amplitude was higher in picrotoxin, likely due to blockade of an overlapping IPSP (Example in E; same cell as C), although, for cells tested with the same stimulation conditions, the increase was not significant (paired $t(3) = 1.58$, $p = 0.21$). Overlapping E/IPSPs produced by field stimulation in MeAd could be from activation of both excitatory and inhibitory MeAd neurons close to the stimulating electrode (see discussion), or via polysynaptic connections. Either could be involved in fine-tuning activity of MePd cells.

Glutamate receptor blockade with kynurenic acid (3 mM) in the bath ($n = 8$) abolished MeAd-induced EPSPs in all the MePd neurons recorded (Fig. 2B,G). Glutamate receptor blockade also decreased the percentage of neurons showing some hyperpolarization with MeAd stimulation from 93.75% in aCSF to 62.5% in kynurenic acid (Fig. 2B), suggesting that some of the evoked IPSPs seen in aCSF were due to poly-synaptic connections. These could possibly be via MePd interneurons activated by glutamatergic MeAd neurons, or via mICNc GABAergic neurons, either of which may synapse onto the recorded MePd neuron. In three neurons recorded under both aCSF and kynurenic acid perfusion, the MeAd induced IPSP was smaller in kynurenic acid (Fig. 2 F), likely reflecting unaffected direct inhibitory connections to MePd from MeAd. The reduction in the mean MeAd-induced IPSP amplitude, however, was not signficant.

3.1.1. Input from MeA to MeP is both excitatory and inhibitory

Chemosensory input from the accessory olfactory bulb is received mainly by MeA and a direct connection from MeA to MeP has been demonstrated anatomically (Maras and Petrulis, 2010b). The direct actions of these connections in terms of their effects on MeP neurons have not been investigated. Here we show with whole-cell recordings of MePd neurons during extracellular field stimulation of MeAd (Fig. 2 A) that MePd receives both excitatory and inhibitory input from MeAd.

3.1.2. Main Intercalated nucleus (mICNc) receives input from MeAd

Whole-cell recordings from mICNc neurons ($n = 21$) showed clear responses to field electrical stimulation of MeAd (Fig. 3 diagram A; summary in B). In aCSF, there were both excitatory (33%) and inhibitory responses (48%) or a complex EPSP/IPSP combination (14%). Fig. 3 C shows a depolarizing response in an mICNc neuron to 25 μA, eliciting an action potential after a small increase in stimulus intensity (Fig. 3D, 30 μA stimulation). Kynurenic acid (3 mM) abolished the depolarization and action potential in the same neuron (Fig. 3E). This effect of Kyn was the same for all MeAd-induced EPSPs in all mICNc neurons tested (Fig. 3B), demonstrating that the MeAd-evoked EPSPs in aCSF are mediated by glutamate. Further, MeAd stimulation during the kynurenic acid bath elicited an inhibitory effect in 43% of mICNc neurons ($n = 7$, Fig. 3B, E), a lower percentage than seen in the aCSF condition (Total inhibitory: 62%) suggesting the presence of some poly-synaptic connections from MeAd to mICNc. Picrotoxin (100 μM) abolished all MeAd-evoked hyperpolarization, leaving 100% of tested neurons with a depolarizing response (Fig. 3B), suggesting all mICNc neurons might receive excitatory connections from MeAd.

3.1.3. MePd inhibited by mICNc

The third connection of the proposed triangular circuit involves inhibition from mICNc to MeP. Whole-cell recordings from MePd neurons in horizontal slices ($n = 22$) during field electrical stimulation of mICNc

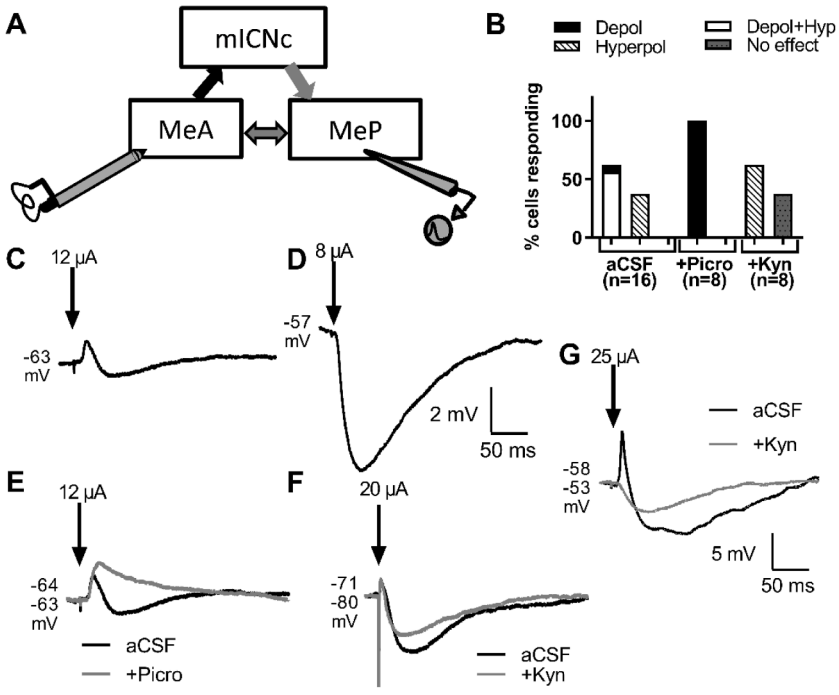

Fig. 2. Projections from MeA to MeP are both excitatory and inhibitory. A) Recording setup with stimulation in MeAd and recording of individual neurons in MePd. B) Percentage of MePd neurons responding to MeAd electrical stimulation in three different bath solutions. 62.5% of neurons responded with an EPSP; with the EPSP followed by an IPSP (C, G) in all but one case. The remaining MePd neurons responded with an IPSP (D). E-G) Examples of current clamp recordings of MePd neurons in slices bathed in aCSF, or aCSF+drug. Blockade of GABAa receptors (picrotoxin, Picro) abolished IPSPs (B, E) and increased the amplitude of EPSPs in some cells (E), although this was not significant. Blockade of glutamate receptors (kynurenic acid, Kyn) abolished EPSPs (G, note difference in scale) and decreased the percentage of MeAd induced IPSPs (B), but the reduction in mean amplitude of IPSPs (e.g., F) was not significant.Extracellular stimulus current shown above arrow in C-G. Cell shown in C, E had zero holding current; cell in F had − 10pA. Resting membrane potentials (RMP) shown to left of each trace. Where two traces are compared (E-G), traces are superimposed with the starting RMP equalized. Actual RMPs are shown to the left with black trace value above, gray below. All RMPs averaged over consecutive sweeps, rounded to the nearest mV; C-F, 10 sweeps; G, 6 sweeps. C and E show the same cell. Of cells contributing to Fig. 2B, aCSF data were from 10 animals, Kyn data from 7 animals and Picro data from 6.

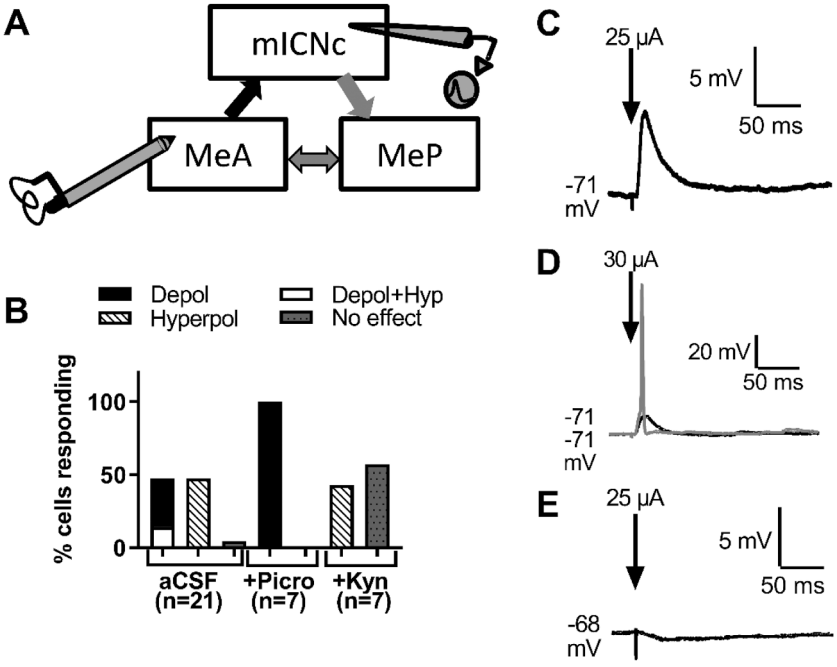

Fig. 3. MeAd projects to mICNc. A) Recording set-up with stimulation in MeAd and recording of individual neurons in mICNc. B) The percentage of mICNc neurons responding to MeAd stimulation in three different bath solutions. C-E) Representative current clamp recordings from one neuron demonstrate the functional excitatory connections from MeAd to mICNc. C) EPSP averaged over 10 sweeps in response to 25 µA stimulation of MeAd in aCSF. D) Action potential firing in the same mICNc neuron with a slightly higher stimulation amplitude in aCSF (30 µA). Black trace = average of 7 sweeps in which no action potential was seen; gray trace shows EPSP and action potential in a representative single sweep from the same neuron (Note different scale from C). E) In the neuron shown in C, D (and in all other neurons tested), kynurenic acid abolished the MeAd-induced EPSP and action potential response. Zero pA holding current for traces in C-E. Extracellular stimulation values indicated above arrows. Of cells contributing to Fig. 3B, aCSF data were from 13 animals, Kyn data and Picro data from 5.

(diagram in Fig. 4A) showed both inhibitory and excitatory effects (Fig. 4B). Since mICNc contains almost exclusively GABAergic neurons, only an inhibitory effect was expected. Most neurons tested in aCSF did show an IPSP (IPSP only: 73%, EPSP followed by IPSP: 18%, Total: 91%). All MePd neurons tested under glutamate blockade (Kyn) were hyperpolarized by mICNc stimulation (n = 10; Fig. 4B). In separate experiments conducted in coronal slices (which do not include the MeA), mICNc stimulation also resulted in a hyperpolarizing response in MePd neurons (e.g. Fig. 4C, black line). If these inhibitory effects are carried by the same pathway in the two types of slices, it would have to traverse the narrow strip of tissue directly connecting mICNc with MeP – which is the only tissue common to the two slice configurations. Of course, the similar effect could have been produced by two different pathways but a direct connection is a simpler explanation. In both horizontal and coronal slices, mICNc-evoked IPSP activity in MePd neurons (n = 7 horizontal; n = 3 coronal) was substantially or completely abolished by the addition of picrotoxin (Fig. 4C, gray line). The effect is clear with Kyn in the bath and no overlapping EPSPs, as in Fig. 4D, where hyperpolarization was significantly reduced (paired $t(2) = 5.36$, $p = 0.033$). Most neurons in the aCSF + picrotoxin bath (without Kyn; horizontal slices) responded to stimulation in mICNc with a depolarization (86%) while only 27% were depolarized in aCSF (EPSP only: 9%, EPSP/IPSP: 18%, n = 22; Fig. 4B). The depolarizing effect seen in some MePd neurons runs contrary to the hypothesized circuit based on the GABAergic phenotype of most mICNc neurons and this may be due to stimulation of fibers of passage, which will be addressed below.

Compared to aCSF alone, the addition of kynurenic acid had no significant overall effect on the amplitude of the mICNc induced IPSP in MePd neurons (paired $t(8) = 1.495$, $p = 0.17$). However, several neurons (67%, n = 9) had a slightly or even a substantially lower IPSP

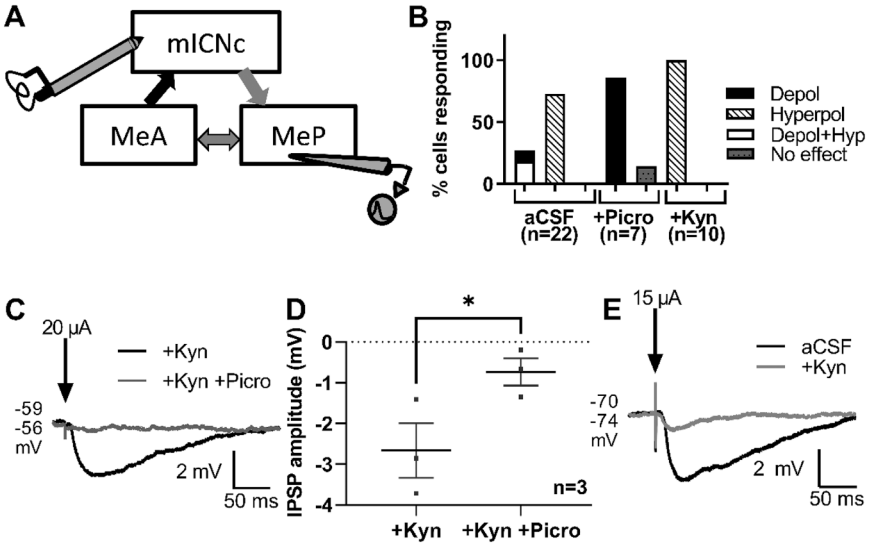

Fig. 4. Functional projections from mICNc to MePd. A) Recording set-up with stimulation electrode in mICNc and recording from neurons in MePd. B) mICNc stimulation elicited IPSPs in most MePd neurons. Picrotoxin essentially eliminated IPSPs, suggesting mICNc projections act mainly via GABAa receptors, but revealed underlying depolarization in some cells which may be due to stimulation of excitatory fibers passing through mICNc en route to MePd (see next section). Kynurenic acid eliminated all depolarizations, including when combined with hyperpolarization, leaving hyperpolarization in 100% of MePd neurons tested. C) In an example cell (without depolarization because the slice was bathed in aCSF + Kyn) the further addition of picrotoxin blocked the IPSP component. D) With glutamate action blocked (+Kyn), picrotoxin significantly reduced mICNc-evoked IPSP amplitude. E) In a few case, Kyn itself reduced IPSP amplitude, possibly by preventing stimulation of MePd interneurons by fibers of passage. D shows Mean + /-SE. * = $p < 0.05$. Cells had zero pA holding current (C,E). Superimposed traces have starting RMPs equalized; actual RMPs to left of traces with black trace RMP above, gray below. Extracellular stimulation values indicated above arrows. Of cells contributing to Fig. 4B, aCSF data were from 17 animals, Kyn data from 8 and Picro data from 5.

amplitude (e.g. Fig. 4E) during glutamate blockade, suggesting that the electrical stimulation may be exciting glutamatergic fibers of passage en route to either additional mICNc neurons or MePd interneurons, producing an indirect inhibitory effect as well as a potential direct excitatory effect in aCSF. Although this indirect connection may be contributing to the strength of the inhibitory effect on MePd, these projections can not be responsible for all, or even a substantial proportion of the inhibitory effect seen in aCSF since all of the MePd neurons recorded under glutamate blockade exhibited an IPSP in response to mICNc stimulation.This robust inhibitory effect suggests that mICNc does indeed have direct GABAergic projections to MePd, consistent with the proposed ICN inhibitory-loop circuit.

In addition to the connections from MeA to mICNc and from mICNc to MeP, all three areas appear to be connected bidirectionally. While not the main focus of the study, these connections clearly could contribute to flexibility/modulation of the circuit and are summarized in supplementary material.

3.1.4. stimulation of mICNc

mICNc is the only one of our three sub-nuclei of interest in which we cannot avoid stimulation close to a substantial fiber bundle; from the intermediate capsule. In order to avoid excitation of these fibers of passage, mICNc was also pharmacologically stimulated using brief, small-volume pulses of L-glutamic acid (10 mM) delivered directly by picrospritzer, through a micropipette (~5uM tip diam.) superficially into mICNc (diagram in Fig. 5 A). The flow path and effectiveness of glutamate delivery was checked in preliminary tests using a micropipette filled with green food coloring (10%) in aCSF, visualizing the flow of fluid from the picospritzer pipette to ensure that the L-glutamic acid in subsequent experiments would flow directly to mICNc, but not MePd.

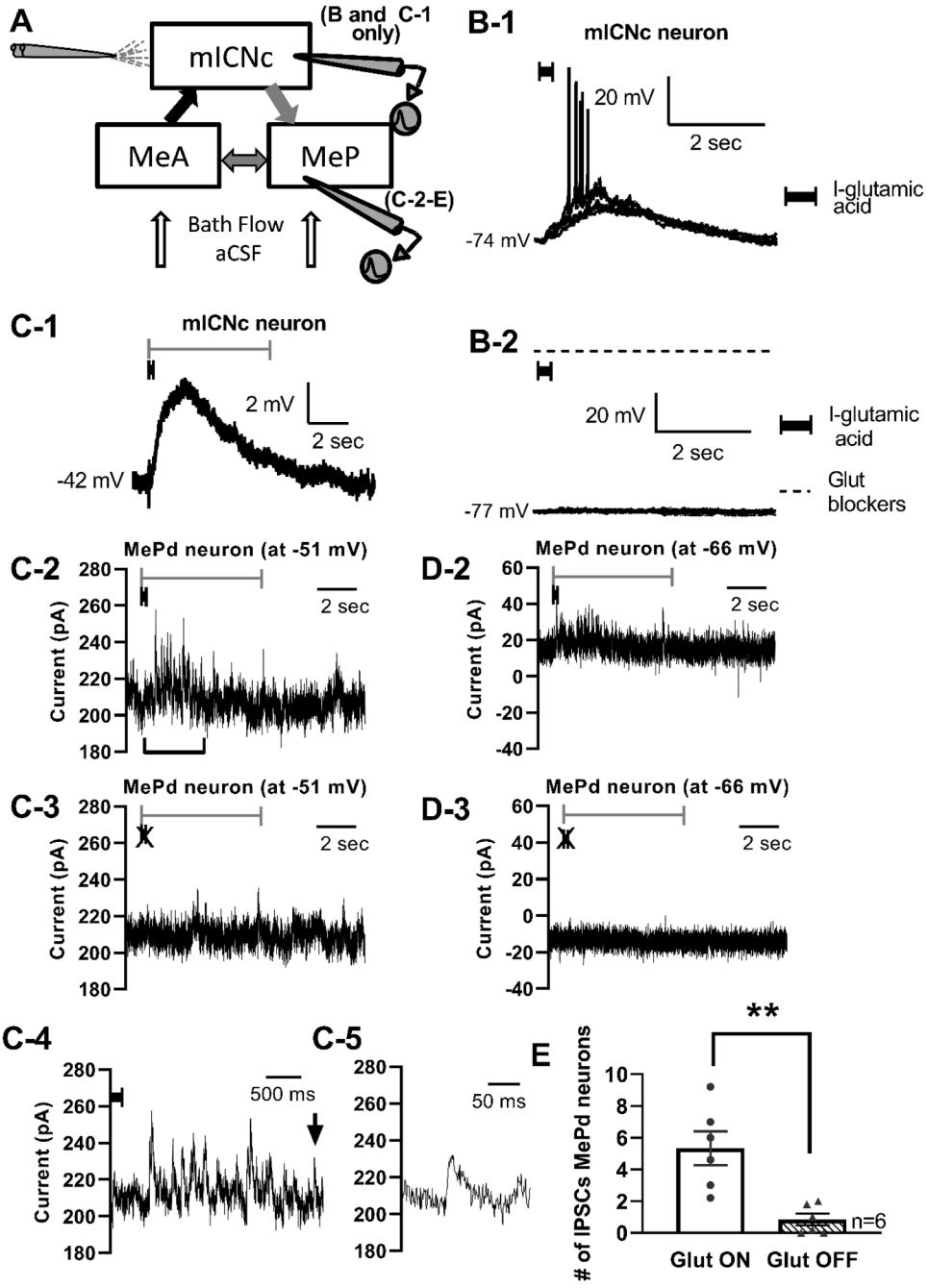

Fig. 5. Pharamacological stimulation of mICNc elicits inhibitory effect on MePd neurons. A) Experimental set-up with local picospritzer puffs of L-glutamic acid used to pharmacologically depolarize and generate action potentials in mICNc neurons over several seconds, without affecting fibers of passage. The effect of mICNc stimulation was recorded in MePd neurons as well as in mICNc. B1 and C1) Current-clamp traces (zero injected current) during puffs of L-glutamic acid (indicated by short black line in B1,C1) producing a depolarization of mICNc neurons (+/- action potentials) that lasted approx. 6 s. B2) With glutamate blockers, Kyn, APV and DNQX in the bath (indicated by dashed line), mICNc depolarization was blocked. C-1) Representative trace from an mICNc neuron in the same slice as the MePd recordings below (C, D). Gray lines indicate the 6 second response time. C2, C3) Voltage clamp recordings were used to visualize small IPSCs (upward deflections) in the same MePd neuron with glutamate-puff delivery either ON (black line, C-2), or with picospritzer on but delivery-line clamped OFF (C-3, crossed black line). D) IPSCs from the same MePd neuron voltage-clamped at a lower membrane potential (−66 mV) were lower in amplitude, consistent with GABA receptor activation and the hyperpolarized reversal potential for chloride. D2 is with glutamate ON; D3 with glutamate OFF (as for C2, C3). C-4 shows the bracketed part of C-2 at faster time-scale; C-5 shows a single IPSC (at the arrow in C-4). E) Mean number of IPSCs during the first 6 ss (in which mICNc neurons were depolarized by a glutamate-puff); with the picospritzer pipette in mICNc tissue and glutamate flow either ON or clamped OFF. In the condition where L-glutamic acid was puffed into mICNc, MePd neurons exhibited a higher number of IPSCs during glutamate delivery (paired-t(5) = 4.13, p = 0.009). (D; Mean +/- SE). The 6 cells contributing to Fig. 5E were from 5 animals.

Recordings from MePd neurons in current clamp while running the picospritzer protocol showed no excitatory effect on MePd neurons from delivery of L-glutamic acid to mICNc. Whole cell, current clamp recordings from mICNc neurons during the same picospritzer protocol were used to determine the time scale of L-glutamic acid excitation and to verify that the concentration.

of L-glutamic acid was sufficient to produce action potential firing in mICNc neurons. Puffs of L-glutamic acid (10 mM, 3.5 p.s.i., 300–500 ms) produced depolarization and action potential spiking in mICNc neurons over approx. a 6 s time course (Fig. 5B-1 and C-1). The effect of the L-glutamic acid puff was abolished by bath application of glutamate receptor antagonists (kynurenic acid: 3 mM, APV: 10 μM, DNQX; 5 μM), demonstrating that the excitatory effect of these very low pressure picospritzer puffs was due to glutamate receptor activation and not due to mechanical disturbance of the slice (Fig. 5B-2). The depolarization elicited by L-glutamic acid puffs in mICNc neurons varied slightly in amplitude and in the number and latency of action potentials elicited (Figs. 5B-1, 5C-1) but was consistent in time course, allowing the inhibitory effect on MePd neurons to be measured as numbers of inhibitory post synaptic currents (IPSCs) observed during the glutamate action. IPSCs are discrete, countable events in voltage clamp recording (see methods and Figs. 5C-4 and 5C-5). Although each should be accompanied by a small IPSP in current-clamp recording, those are more drawn out, asynchronous upon repetition, as are IPSCs, but overlapping and thus more difficult to quantify in current clamp traces during these experiments.

Voltage clamp recordings from MePd neurons during pharmacological excitation of mICNc by L-glutamic acid puffs (Fig. 5 A) verified the inhibitory effect on MePd of mICNc stimulation without the unintended excitation of fibers of passage. Fig. 5C-1 shows depolarization of an mICNc neuron by pharmacological stimulation with the Picospritzer micropipette placed in mICNc. The same Picospritzer protocol elicited a higher number of IPSCs in an MePd neuron voltage clamped at − 51 mV (Fig. 5C-2) and at − 66 mV (Fig. 5D-2), compared to recordings obtained from the same MePd neuron at the same holding potentials (−51 mV or −66 mV), when the picospritzer flow-tube was clamped shut (Fig. 5C-3; 5D-3). Overall, there was a significant increase in the number of IPSCs in 6 MePd neurons in the 6 ss after an L-glutamic acid puff in mICNc, compared to 6 s after a Picospritzer pulse with glutamate flow shut OFF (Fig. 5E) (paired-t(5) = 4.13, p = 0.009). For this analysis, MePd neurons were held between − 50 and − 66 mV and the holding voltage was consistent for each neuron across conditions. IPSCs were appropriately larger at depolarized potentials (Fig. 5C-2 compared to 5D-2) consistent with GABA receptor activation and the hyperpolarized chloride reversal potential (~ −124 mV). These data suggest that the inhibitory effect of mICNc stimulation on MePd neurons is indeed due to activation of mICNc neurons and not substantially attributable to the electrical stimulation of fibers of passage.

3.2. Modulation by dopamine; effect of dopamine on the mICNc – MePd circuit

3.2.1. Dopamine inhibits mICNc

Dopamine inhibits ICN cells via a D1 action in other species and could potentially affect transmission through the mICNc loop-pathway investigated here in hamster. Dopamine hydrochloride (DA, 30 μM) was used to assess a DA-ergic effect on mICNc activity and transmission (schematic in Fig. 6 A). Data were collected using whole-cell current-clamp from cells in coronal slices bathed in aCSF which was then replaced by the same solution with added DA for 5 min, followed by a 30 min washout of DA with the original aCSF baseline solution. Values given are averaged over the last three 50 s sweeps of each bath, before switching to a new bath. These mICNc cells are small and patch recording stability is difficult to maintain for prolonged periods, so access resistance was checked periodically (see methods) to ensure that only data from cells that remained healthy throughout the experiment were included in the analysis (Fig. 6B-F). The addition of DA to the aCSF bath hyperpolarized all 7 cells tested (Fig. 6B), for a significant decrease in mean resting membrane potential (RMP). Four of the seven cells (DA responsive) returned close to or above their original CSF-baseline RMP on washout but three cells showed a further decline in RMP and overall, washout produced a small, non-significant return towards aCSF baseline (one way RM ANOVA, F (1.26, 7.54) = 5.61, p = 0.042, Tukey post-hoc: aCSF vs DA: p = 0.0023; aCSF vs Washout: p = 0.1; DA vs washout: p > 0.9). Five of the seven cells also showed a decrease in membrane resistance in the DA bath. Group-mean membrane resistance (Fig. 6 C) decreased slightly but non-significantly with DA but rose significantly from DA levels upon washout (one way RM ANOVA, F(1.3, 7.81) = 9.357, p = 0.013, Tukey post-hoc: aCSF vs DA: p = 0.87; aCSF vs washout: p = 0.079; DA vs washout p = 0.008). The mean number of

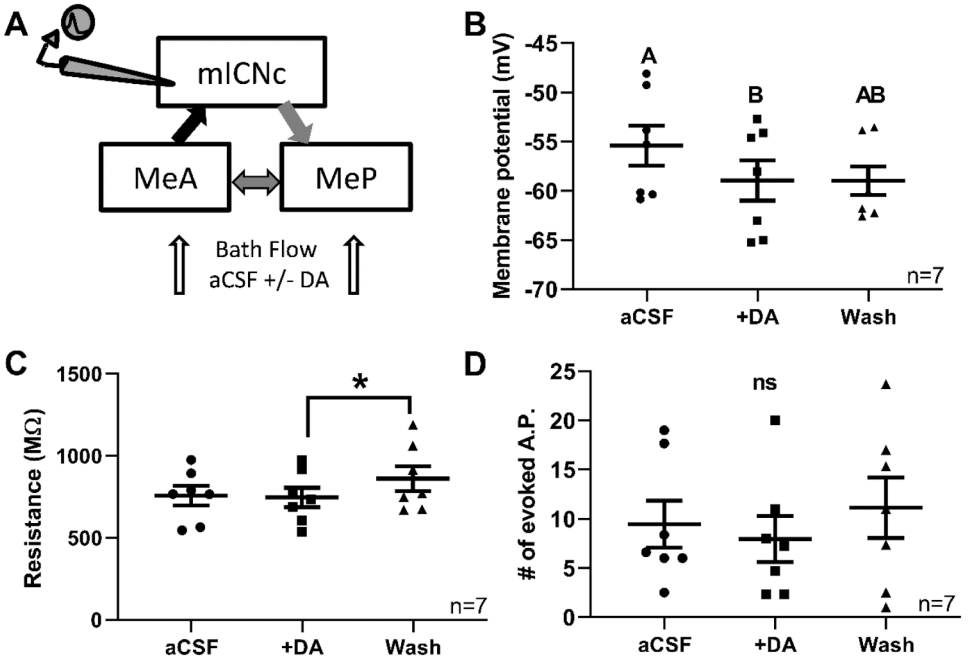

Fig. 6. Suppressive effect of dopamine on mICNc neurons. A) Schematic: Bath applied dopamine-HCl (DA) depressed the membrane potential and excitability of mICNc neurons. B) In seven cells initially bathed in aCSF, adding DA significantly decreased mean resting membrane potential (RMP), with a washout value not significantly different from baseline but not fully recovered. C) Mean decrease in membrane resistance in DA was small but with a larger upward shift on washout. D) The mean number of action potentials elicited by a standard intracellular depolarization pulse was clearly reduced in the presence of DA in several cells, but not significantly in the group. An example of a strongly responsive cell is shown in supplemental Fig S2.,. Data indicated by different superscript letters or an asterisk are significantly different, p < 0.05. Data for Fig. 6B-D were from 5 animals. All cells had zero holding current.

action potentials elicited by a standard intracellular depolarization (Fig. 6D), also decreased with DA but not significantly (one way RM ANOVA, $F(1.42, 8.62) = 1.75$, $p < 0.2$). Intracellular current injection was 20 – 100 pA, standardized for each cell as the minimal current eliciting reliable action potential firing. Three of the cells tentatively labeled "DA responsive" for RMP depression and recovery also showed the expected decline and recovery of membrane resistance and two showed the same pattern for decline and recovery of evoked action potential number. However, these consistent performers are too few to posit the existence of two populations. These mICNc neurons had a relatively low level of baseline firing so the lack of significance may be due to a floor effect. Supplemental Fig. S2 shows the time course of the resistance change and decrease in evoked action potentials for one of the more strongly responsive cells.

Although generally consistent with the opening and reclosing of channels in a dopamine dependent manner, the DA effect on membrane potential and resistance here is uneven with some individual cells showing a larger DA effect. The effect of DA on mICNc inhibition of MePd (see below), however, is unambiguous and consistent with a suppressive effect of DA on mICNc.

3.2.2. *Dopamine decreases mICNc induced inhibition of MePd*

As shown above (Fig. 4), stimulation of mICNc elicits a brief GABAa-receptor-sensitive hyperpolarization of MePd neurons. To assess whether DA can modulate MePd activity via its effect on mICNc, the responses of MePd neurons to mICNc stimulation were recorded during DA bath application and during DA washout, in coronal slices (Fig. 7A). Hyperpolarization of mICNc neurons occurs between 5 and 7 min after the start of DA application (supplemental Fig. 2 A) so MePd responses were analyzed beginning six minutes after the start of the DA bath (approx. 7 min after the initial baseline recording). To reduce circuit-level effects and focus on the effect of DA on GABAergic input from mICNc to MePd, these recordings were performed under comprehensive glutamate receptor blockade [3 mM kynurenic acid, APV (10 μM) and DNQX (5 μM)]. Baseline responses were collected 2–5 min into the glutamate receptor antagonist perfusion. Whole cell current clamp recordings were collected from six MePd neurons, with extracellular stimulation in mICNc. DA application (Fig. 7B) significantly decreased the amplitude of the hyperpolarization elicited in MePd cells by stimulation of mICNc, with significant recovery on washout (One-way RM ANOVA: $F(1.65, 8.25) = 10.23$, $p = 0.0072$; Tukey post-hoc: Baseline vs DA: $p = 0.038$; Baseline vs Washout: $p = 0.92$; DA vs Washout: $p = 0.01$). Representative traces from one MePd neuron are shown in Fig. 7 C. After washout of DA (but not glutamate receptor antagonists), the amplitude of the mICNc-evoked IPSP returned to pre-DA baseline levels. Resting membrane potentials are somewhat variable over extended current clamp recording sessions, with this cell at somewhat lower RMP level after 30 min of washout. However, DA did not appear to affect the MePd neurons directly since DA application had no systematic or significant effect on the resting membrane potential of MePd neurons (One-way RM ANOVA: $F(1.5, 7.511) = 2.94$, $p = 0.12$, Fig. 7D).

3.2.3. *Activation of dopamine D1 receptors has no effect on mICNc inhibition of MePd*

Work in other species demonstrated a DA-ergic inhibition of ICN cells via a DA-D1 mechanism (Gregoriou et al., 2019; Marowsky et al., 2005) but we could not confirm this finding with mICNc cells in hamster. The same DA-D1 receptor agonist used in previous studies, at the same concentration (Dihydrexidine; DHX, 2 μM; Marowsky et al., 2005) did not inhibit hamster mICNc neurons (see next section and Fig. 8, below). Additional experiments investigated the ability of the DA-D1 agonist to affect of hyperpolarization of MePd neurons elicited by mICNc stimulation (Fig. 7 A). All MePd neurons tested (n = 8) showed the expected hyperpolarization elicited by mICNc stimulation during glutamate receptor blockade (3 mM kynurenic acid in aCSF). The amplitude of MePd hyperpolarization recorded 5–10 min after the addition of DHX (2 μM)

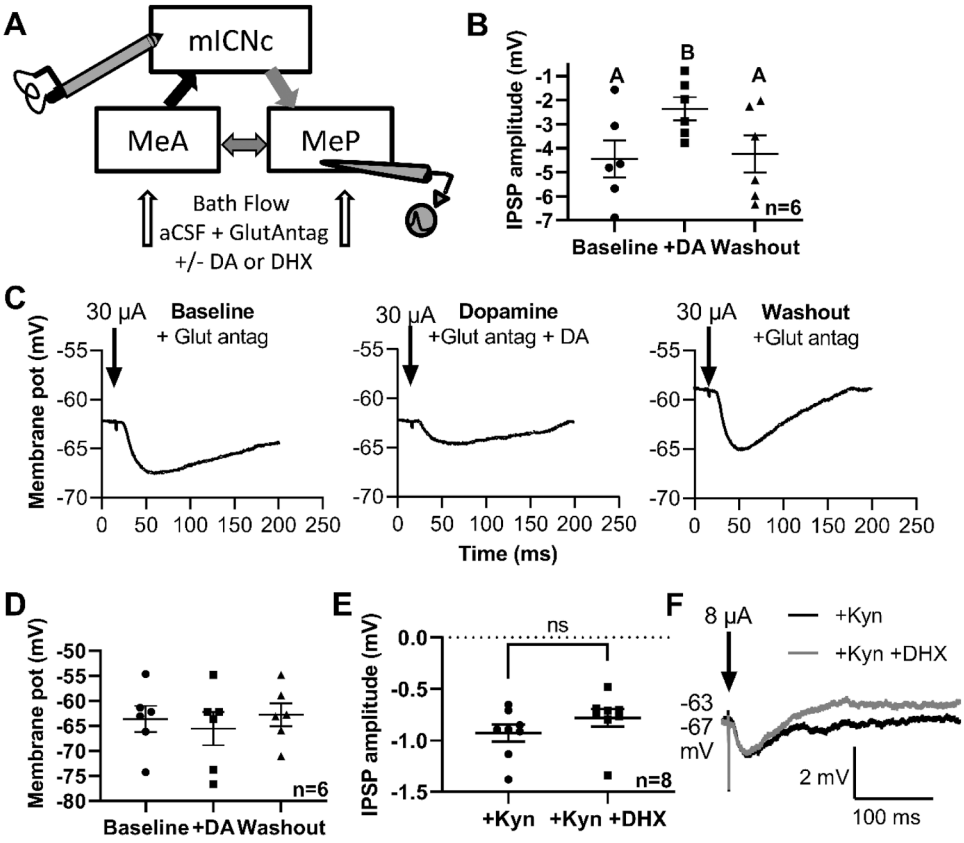

Fig. 7. DA but not DHX reduces hyperpolarizing effect of mICNc on MePd neurons. A) Schematic: Neurons recorded in MePd; Extracellular stimulation in mICNc, in slices continuously perfused with a glutamate receptor antagonist mix (kynurenic acid: 3 mM, APV: 10 μM, DNQX: 5 μM, in aCSF). Dopamine (DA; DA-HCl, 30 μM) was added to the glutamate antagonist bath and then washed out with aCSF+glutatmate receptor antagonists. B) DA significantly decreased the mean amplitude of the mICNc driven hyperpolarization (plotted downward) compared to baseline (aCSF and glutamate antagonists only), with a return to baseline levels upon DA washout. C) Representative traces show the IPSP amplitude in the three bath conditions in the same MePd neuron. D) Dopamine did not have a signficant direct effect on the resting membrane potential of MePd neurons. E) The DAD1 receptor agonist, dihydrexidine (DHX; 2 μM) had no significant effect on mean mICNc-driven IPSP amplitude in MePd neurons during glutamate blockade by Kyn; representative trace in F. Traces in C are an average of 10 consecutive sweeps. B -E show mean values + /- SE. All traces had zero pA holding current. F-traces are superimposed with RMP equalized; actual RMP values at left with black-trace, RMP value on top, gray trace value below. Stimulation amplitude noted above arrows. Significant differences in B are indicated by different superscript letters. Data for Figs. 7B and 7D were from 4 animals. Data for Fig. 7E were from 5 animals.

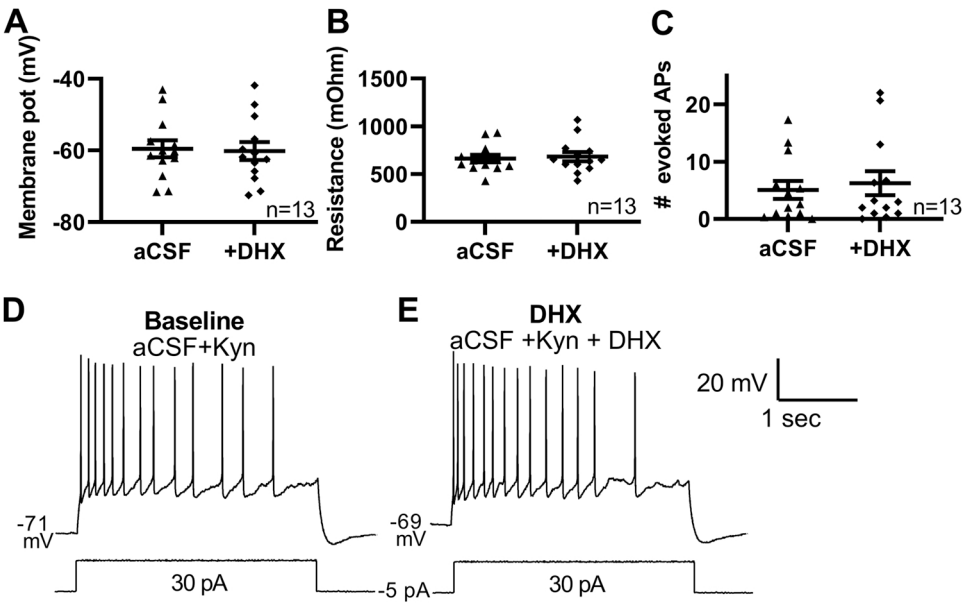

Fig. 8. Effect of dopamine D1 receptor activation on mICNc neurons. Recording set-up as in Fig. 6, with DHX replacing DA. A-C) The DAD1 receptor agonist, dihydrexidine (DHX; 2 μM) had no significant effect on mICNc neurons. In 13 cells, DHX had no significant effect on mean resting membrane potential (A), input resistance (B) or number of action potentials evoked by standard depolarization (C). D-E) Representative traces of evoked action potential firing in a mICNc neuron during baseline and DHX bath perfusion (−5 pA holding current, with 3 s, 30 pA intracellular depolarizing current). (A-C show mean +/- SE). Data for Fig. 8 A-C were from 5 animals (13 slices).

to the bath during glutamate receptor blockade was not significantly different from that before DHX, (paired t (7) = 1.29, p = 0.2 Mean values are shown in Fig. 7E; an example in Fig. 7 F). Due to the lack of a DHX effect and the long (more than 30 min) washout time for DHX (Gorelova et al., 2002), washout data were not collected for all cells and, thus, were not included in the analysis. Because kynurenic acid (3 mM) had proved to be effective in suppressing all spontaneous EPSPs in MePd cells and reducing spontaneous IPSPs (See supplementary Fig. S4), Kyn alone was used to block potential glutamate-mediated circuit effects in these DHX experiments.

3.2.4. *Dopamine D1 agonist DHX has no effect on mICNc neurons*

Consistent with the lack of DAD1 effect on mICNc induced hyperpolarization of MePd neurons (Fig. 7E-F), bath applied DHX had no clear effect on mICNc neurons. Overall, there was no significant effect of DHX (n = 13) on resting membrane potential (paired t (12) = 1.08, p = 0.3), membrane resistance (paired t (12) = 1.38, p = 0.19) or number of evoked action potentials (paired t (12) = 1.58, p = 0.14; Fig. 8A-C). The quality of recordings from these small mICNc neurons is shown in Fig. 8D, E (with no decrease in firing under DHX) as well as in Fig. S2.

DA but not DHX consistently decreased membrane potential in mICNc cells of the same slice. The supplemental material shows that mICNc neuron sensitivity to DA can be seen even when DA-D1 agonist was ineffective. These agents were applied serially to the same cells in slices treated with tetrodotoxin (TTX) in the bath to prevent action potential firing, reduce circuit level influences and confine results mostly to direct effects on the recorded cell (Fig S3).

DA decreased membrane potential in mICNc neurons that were unresponsive to DHX (Fig S3C,D). Fig S3C shows a substantial hyperpolarizing change from TTX-bath baseline during DA/TTX treatment although the preceding DHX/TTX treatment was ineffective. Fig. S3D shows the steep hyperpolarization by DA in a cell unaffected by DHX. These results suggest that the effect of DA on mICNc neurons shown previously (Fig. 6) is not mediated by activation of DAD1 receptors, at least not by DHX at the dose used in other studies (Marowsky et al., 2005).

4. Discussion

We present here evidence for the three functional connections necessary for a proposed modulatory and regulatory action of the amygdala main-intercalated nucleus cells during chemosensory social signaling. These connections constitute a circuit potentially influencing behavioral and physiological responses to social signals and may be sensitive to modulation by brain state via dopamine and cortical input. The circuit is analogous to those proposed for the medial intercalated cell group regulating fear conditioning and extinction (Duvarci and Pare, 2014; Marowsky et al., 2005). The inputs and outputs are different but the transaction between intercalated cells, their adjacent major amygdaloid nuclei and various modulatory systems appear to be similar. The intercalated nuclei (ICNs), also called intercalated cells (ITCs) or intercalated masses (IMs) are small groups of small predominantly GABAergic cells interspersed between the principal amygdaloid nuclei. Various functions for the intercalated nuclei (ICN) cell-groups have recently been investigated, as discussed further below.

In the social communication circuit, chemosensory information from the main and accessory olfactory bulbs, traverses anterior (MeA) and posterior (MeP) medial amygdala en route to basal forebrain (Been and Petrulis, 2011). Different chemosignals generate different MeA and MeP patterns of activity (Meredith and Westberry, 2004; Westberry and Meredith, 2016, 2017, Samuelsen and Meredith, 2009, Bergan et al., 2014). Transmission from both areas to basal forebrain combine to elicit appropriate behavioral and physiological responses (Been and Petrulis, 2011; Maras and Petrulis, 2010b). We show here both excitatory and inhibitory connection from MeA to MeP, as we might expect if MeA input is further processed in MeP. As suggested by our previous IEG response data (Meredith and Westberry, 2004), we also show a second indirect pathway from MeA to MeP via cells of the caudal main Intercalated Nucleus (mICNc), which lies adjacent to MeP. MeA has excitatory inputs to mICNc and mICNc is predominantly inhibitory to MeP. This pathway is sufficient to modulate the patterns generated by direct MeA to MeP transmission and, thus, potentially alter overall response and MeA/P output to basal forebrain. The chemosensory pathway through medial amygdala is critical for appropriate physiological and behavioral responses to reproductive and social signals in rodents and most mammals (Newman, 1999; Petrulis, 2013). That it should be modulated according to internal state and other input is not surprising. The circuit documented is similar to those important for modulation of other affective/ motivational mechanisms (Hagihara et al., 2021). Behaviors motivated by social chemosensory signals are not automatic; for example, they need to be suspended or altered in the presence of danger or competing motivations. Selective mICNc inhibition of MeP neurons may reduce medial amygdala output or alter its pattern to provide this necessary flexibility of response when a given chemosensory signal is

encountered under different circumstances.

The evidence for anatomical connections from ICN to MeP and MeA is clear although sparsely documented in the literature (rat: Mańko et al., 2011; cat: Paré and Smith, 1993). Our electrophysiological data, here, strongly support functional connections based on activation and/or inhibition of neurons in one amygdala region by electrical stimulation in another. These experiments were conducted in hamsters, the species in which we have evidence for mICNc involvement in chemosensory processing (Meredith and Westberry, 2004; Westberry and Meredith, 2016).

Extracellular electrical stimulation such as we use activates nearby cells largely via the dense sodium channel region of the initial axonal segment (IAS) close to the soma. Myelinated axons also have dense sodium channel regions at the nodes of Ranvier and could be activated antidromically, possibly resulting in distant effects via their axon collaterals. Medial amygdala, however, has only a few thin myelinated axons (Hermel et al., 2006) and we did not place stimulating electrodes close to surrounding fiber tracts (except possibly near mICNc, see below). Unmyelinated neurons also have regions of high sodium channel density close to the soma but sodium channel density decreases distally along the axon, raising the threshold for activation (e.g.: hippocampal granule cells; Schmidt-Hieber and Bischofberger, 2010). There are exceptions, such as the fast spiking hippocampal basket-cell interneurons, which maintain a high sodium channel density along the axon to ensure rapid inhibitory action on their targets (Hu and Jonas, 2014). No similar cells are reported for medial amygdala but in any case such local interneurons would not directly influence neurons outside the stimulated nucleus. Thus, the spatially restricted and steep voltage gradient produced by a low current from a bipolar electrode is most likely to influence neighboring nuclei via activation of IAS regions of nearby cells, generating orthodromic action potentials. Antidromic activation is not ruled out but is unlikely to be a major contributor to the data. In an extensive analysis of electrical stimulation in the retina, which has both myelinated (ganglion cell) and unmyelinated (bipolar cell) excitable axons, Rattay et al. (Rattay et al., 2017) estimated thresholds for IAS stimulation by an electrode at 50 μm distance to be in the general range of currents we used here (for retinal neurons of both types). Of our stimulation sites, only those in mICNc are close to substantial fiber bundles (from the intermediate capsule). However, we show that our proposed inhibitory connection from mICNc to MePd can be activated by local glutamate release in mICNc so does not rely on antidromic or en-passant axon activation. This connection is likely to be direct as very similar results are obtained for the inhibition of MeP cells by mICNc stimulation in both horizontal and coronal slices. If not direct, the similar functional connections would have to be via two very different pathways. The only connection pathway available in both slice-types would be within the 350 μm x 350 μm column of tissue directly between the two nuclei; the only tissue intact in both slice orientations.

Inhibition from ICN cell groups can suppress or modulate activity in their adjacent larger amygdala nuclei, as observed in the fear conditioning circuit. These ICN effects are themselves subject to inhibition by dopamine or enhancement via cortical circuits, allowing an adaptation to ongoing brain state. From reports of its action in the paracapsular ICN cell-groups in the fear conditioning circuit in mouse and in rat (Gregoriou et al., 2019; Marowsky et al., 2005), we expected dopamine might have a D1 receptor-dependent inhibitory effect on mICNc in hamsters. We confirmed the dopamine suppression of mICNc inhibition of MeP but could not confirm a D1 mechanism. There may be a species difference in receptor sensitivity but there does seem to be a potential mechanism for dopamine to modulate amygdala ICN processing in the hamster, as in the mouse and rat. The triangular circuit we report here for the chemosensory pathway can modulate neural response to sensory input and itself be regulated by dopamine. As in other circuits with an ICN-loop, DA inhibition could allow for switching amygdala processing to a more automatic mode, less sensitive to cortical input. We have no direct evidence for cortical excitation of mICNc but it is a feature of other ICN circuits. Cortical excitation could impose an inhibition on MeP, interrupting or modifying the physiological/behavioral consequences of chemosensory input through MeA/P.

Some of the first evidence for distinct intercalated cell-group circuits and functions was in fear conditioning and its extinction. The medial paracapsular cell-group receives excitatory input from the lateral/basolateral (La/BLA) amygdaloid nuclei and in turn can suppress output from the central nucleus (Ce) (Duvarci and Pare, 2014), reducing freezing behavior after extinction of previously fear-conditioned stimuli. This pathway opposes the direct pathway from BLA to Ce which initially induces freezing. Both pathways are subject to regulation by cortical input, dopamine and neuropeptides (Thompson and Neugebauer, 2017), particularly by modulation of the ICN limb of the circuit. Similar BLA to Ce direct and indirect (ICN) pathways, but via the main intercalated cell group, are also implicated in regulation of fear, pain and anxiety (Winters et al., 2017). A different pathway, from anterior olfactory nucleus to the lateral paracellular ICN group, appears to be active in reducing stress during conditioned fear when social contact with a conspecific of the same strain is possible (Minami et al., 2019). Projections to ICN cell groups from prefrontal cortex in rats (Amano et al., 2010; Amir et al., 2011) are potentially involved in fear conditioning and extinction. In primates, direct cortical projections to the central nucleus, and indirect pathways via the intercalated cell masses also appear to be critically involved in regulating autonomic arousal associated with emotion and anxiety. Anterior cingulate cortex favors arousal but a powerful connection from posterior orbitofrontal cortex to the intercalated cells can lead to inhibition of Ce output, suppressing arousal and potentially reducing anxiety (Zikopoulos et al., 2017). The ICN link in this circuit is subject to dopamine inhibition however, and Zikopoulos et al. (2017) suggest that high DA levels could override cortical control of this pathway, as in anxiety disorders. DA, in this context, appears to have a general effect on ICN influence; other modulators may be more discrete. Endogenous opiates can influence ICN function and affect behavior (Gregoriou et al., 2019; Likhtik et al., 2008). They can also be released by ICN cells themselves to influence specific synapses selectively (Winters et al., 2017). These data show the importance of ICN cell groups in modulating behavioral responses based on cortical input and the animal's brain-state. A similar role of mICNc may be to modulate activity in medial amygdala during chemosignal processing, thus modulating behavioral responses to various chemosignals.

The proposed triangular circuit between MeA and MeP, with feedforward inhibition through mICNc provides a mechanism for modulation of behavioral response but is not the only pathway between these nuclei; as explored further in supplementary material. MeA and MeP are connected by projections in both directions, as expected (Maras and Petrulis, 2010b, 2010c, 2010a) and include both excitation and inhibition. Also as expected, mICNc connections to MeP seem primarily inhibitory, but there is also inhibition of MeA; in both cases consistent with the overwhelmingly GABA-ir nature of ICN neurons. Some depolarizing effects in MeP (and MeA), from stimulation in mICNc, appear to be largely or fully explained by fibers of passage, in or around mICNc, probably from intermediate capsule (Mańko et al., 2011), although polysynaptic connections including disinhibition may also occur. In as far as MeA can influence MeP through ICN as well as directly, and MeP can also influence MeA, there are multiple pathways for generation of characteristic patterns of response in both MeA and MeP. These inputs build on the basic activity-templates for chemosensory input and provide a range of input patterns to basal forebrain, which may be expected to evoke different adaptive behavioral and physiological responses. Selective activation or suppression of mICNc by optogenetic or chemogenetic means in behaving animals might help to test this prediction but to date are not easily exploited in hamsters.

The ICN circuits in fear, anxiety and pain mechanisms involve branches of sensory input from auditory, visual and somatosensory pathways to the amygdala providing emotional/motivational context

for environmental input to influence internal state (e.g., Asede et al., 2015; Thompson and Neugebauer, 2017). A similar involvement of ICN cells with social communication is proposed here. It would be consistent with the effects of genetic disruption of the development of ICN-cell precursors (Kuerbitz et al., 2018), which leads to deficits in social behavior as well as fear extinction.

It is tempting to speculate that the confluence of non-chemo-sensory pathways to the amygdala may have evolved to integrate social chemosensory information available there, with more generalizable sensory information that is not necessarily specific to the needs of reproduction, competition and predator avoidance. If so, the ICN-based circuit module described here for the chemosensory pathway may be the more ancient; later co-opted for regulation of fear conditioning and a variety of functions in the emotional/motivational realm not directly involved in social communication; and possibly in a rather precise manner (Strobel et al., 2017; Winters et al., 2017).

5. Conclusion

The triangular circuit we demonstrate here involving an ICN-loop modulates the chemosensory pathway from main and accessory bulbs to basal forebrain, important for social communication. Whether there is a direct cortical influence as seen for other such ICN-loops is not known but extra-amygdaloid input may fine-tune chemosensory-information flow via this circuit. Its DA sensitivity could also have a more general adaptive function; switching amygdala processing to and from a more automatic mode, less or more sensitive to cortical input.

Contributions

LMB and MM planned the experiments and data analysis; LMB performed the experiments and analyzed the data, LMB and MM wrote the paper.

Conflict of interest

The authors declare no conflicts of interest.

Acknowledgements

The authors thank Nicholas Thiebaud, John Cortell and Brendan Biggs for advice and helpful discussions. The work was supported by NIH grants R01 DC005813 and Chemosensory Training Grant T32 DC00044, from NIDCD.

Appendix A. Supporting information

Supplementary data associated with this article can be found in the online version at doi:10.1016/j.ibneur.2022.01.005.

References

Adolphs, R., 2010. What does the amygdala contribute to social cognition? Ann. NY Acad. Sci. 1191, 42–61.
Amano, T., Unal, C.T., Paré, D., 2010. Synaptic correlates of fear extinction in the amygdala. Nat. Neurosci. 13, 489–494.
Amir, A., Amano, T., Pare, D., 2011. Physiological identification and infralimbic responsiveness of rat intercalated amygdala neurons. J. Neurophysiol. 105, 3054–3066.
Asede, D., Bosch, D., Lüthi, A., Ferraguti, F., Ehrlich, I., 2015. Sensory inputs to intercalated cells provide fear-learning modulated inhibition to the basolateral amygdala. Neuron 86, 541–554.
Been, L.E., Petrulis, A., 2011. Chemosensory and hormone information are relayed directly between the medial amygdala, posterior bed nucleus of the stria terminalis, and medial preoptic area in male Syrian hamsters. Hormon. Behav. 59, 536–548.
Bergan, J.F., Ben-Shaul, Y., Dulac, C., 2014. Sex-specific processing of social cues in the medial amygdala. ELife 3.
Biggs, L.M., Meredith, M., 2020. Activation of calcium binding protein-ir neurons in medial amygdala during chemosignal processing. Chem. Sens. 45, 439–448.
Billing, A., Henrique Correia, M., Kelly, D.A., Li, G.-L., Bergan, J.F., 2020. Synaptic connections of aromatase circuits in the medial amygdala are sex specific. ENeuro 7 (3), 2020.
Cádiz-Moretti, B., Otero-García, M., Martínez-García, F., Lanuza, E., 2016. Afferent projections to the different medial amygdala subdivisions: a retrograde tracing study in the mouse. Brain Struct. Funct. 221, 1033–1065.
Carvalho, V.M., de, A., Nakahara, T.S., Souza, M.A., de, A., Cardozo, L.M., Trintinalia, G. Z., Pissinato, L.G., Venancio, J.O., Stowers, L., Papes, F., 2020. Representation of olfactory information in organized active neural ensembles in the hypothalamus. Cell Rep. 32, 108061.
Carvalho, V.M.A., Nakahara, T.S., Cardozo, L.M., Souza, M.A.A., Camargo, A.P., Trintinalia, G.Z., Ferraz, E., Papes, F., 2015. Lack of spatial segregation in the representation of pheromones and kairomones in the mouse medial amygdala. Front. Neurosci. 9.
Coolen, L.M., Wood, R.I., 1998. Bidirectional connections of the medial amygdaloid nucleus in the Syrian hamster brain: simultaneous anterograde and retrograde tract tracing. J. Comp. Neurol. 399, 189–209.
Demir, E., Li, K., Bobrowski-Khoury, N., Sanders, J.I., Beynon, R.J., Hurst, J.L., Kepecs, A., Axel, R., 2020. The pheromone darcin drives a circuit for innate and reinforced behaviours. Nature 578, 137–141.
Duvarci, S., Pare, D., 2014. Amygdala microcircuits controlling learned fear. Neuron 82, 966–980.
Gorelova, N., Seamans, J.K., Yang, C.R., 2002. Mechanisms of dopamine activation of fast-spiking interneurons that exert inhibition in rat prefrontal cortex. J. Neurophysiol. 88, 3150–3166.
Gregoriou, G.C., Kissiwaa, S.A., Patel, S.D., Bagley, E.E., 2019. Dopamine and opioids inhibit synaptic outputs of the main island of the intercalated neurons of the amygdala. Eur. J. Neurosci. 50, 2065–2074.
Hagihara, K.M., Bukalo, O., Zeller, M., Aksoy-Aksel, A., Karalis, N., Limoges, A., Rigg, T., Campbell, T., Mendez, A., Weinholtz, C., et al., 2021. Intercalated amygdala clusters orchestrate a switch in fear state. Nature 594, 403–407.
Hermel, E.E.S., Faccioni-Heuser, M.C., Marcuzzo, S., Rasia-Filho, A.A., Achaval, M., 2006. Ultrastructural features of neurons and synaptic contacts in the posterodorsal medial amygdala of adult male rats. J. Anat. 208, 565–575.
Hu, H., Jonas, P., 2014. A supercritical density of Na(+) channels ensures fast signaling in GABAergic interneuron axons. Nat. Neurosci. 17, 686–693.
Kang, N., Baum, M.J., Cherry, J.A., 2009. A direct main olfactory bulb projection to the "vomeronasal" amygdala in female mice selectively responds to volatile pheromones from males. Eur. J. Neurosci. 29, 624–634.
Kang, N., McCarthy, E.A., Cherry, J.A., Baum, M.J., 2011a. A sex comparison of the anatomy and function of the main olfactory bulb-medial amygdala projection in mice. Neuroscience 172, 196–204.
Kang, N., Baum, M.J., Cherry, J.A., 2011b. Different profiles of main and accessory olfactory bulb mitral/tufted cell projections revealed in mice using an anterograde tracer and a whole-mount, flattened cortex preparation. Chem. Sens. 36, 251–260.
Keshavarzi, S., Sullivan, R.K.P., Ianno, D.J., Sah, P., 2014. Functional properties and projections of neurons in the medial amygdala. J. Neurosci. 34, 8699–8715.
Kondo, Y., Arai, Y., 1995. Functional association between the medial amygdala and the medial preoptic area in regulation of mating behavior in the male rat. Physiol. Behav. 57, 69–73.
Kuerbitz, J., Arnett, M., Ehrman, S., Williams, M.T., Vorhees, C.V., Fisher, S.E., Garratt, A.N., Muglia, L.J., Waclaw, R.R., Campbell, K., 2018. Loss of intercalated cells (ITCs) in the mouse amygdala of tshz1 mutants correlates with fear, depression, and social interaction phenotypes. J. Neurosci. 38, 1160–1177.
Lehman, M.N., Winans, S.S., 1982. Vomeronasal and olfactory pathways to the amygdala controlling male hamster sexual behavior: Autoradiographic and behavioral analyses. Brain Res. 240, 27–41.
Likhtik, E., Popa, D., Apergis-Schoute, J., Fidacaro, G.A., Pare, D., 2008. Amygdala intercalated neurons are required for expression of fear extinction. Nature 454, 642–645.
Lin, H., Müller-Bardorff, M., Gathmann, B., Brieke, J., Mothes-Lasch, M., Bruchmann, M., Miltner, W.H.R., Straube, T., 2020. Stimulus arousal drives amygdalar responses to emotional expressions across sensory modalities. Sci. Rep. 10, 1898.
Mańko, M., Geracitano, R., Capogna, M., 2011. Functional connectivity of the main intercalated nucleus of the mouse amygdala. J. Physiol. 589, 1911–1925.
Maras, P.M., Petrulis, A., 2006. Chemosensory and steroid-responsive regions of the medial amygdala regulate distinct aspects of the opposite-sex odor preference in male syrian hamsters. Eur. J. Neurosci. 24, 3541–3552.
Maras, P.M., Petrulis, A., 2010a. The anterior medial amygdala transmits sexual odor information to the posterior medial amygdala and related forebrain nuclei. Eur. J. Neurosci. 32, 469–482.
Maras, P.M., Petrulis, A., 2010b. Anatomical connections between the anterior and posterodorsal sub-regions of the medial amygdala: integration of odor and hormone signals. Neuroscience 170, 610–622.
Maras, P.M., Petrulis, A., 2010c. Lesions that functionally disconnect the anterior and posterodorsal sub-regions of the medial amygdala eliminate opposite-sex odor preference in male Syrian hamsters (Mesocricetus auratus). Neuroscience 165, 1052–1062.
Marowsky, A., Yanagawa, Y., Obata, K., Vogt, K.E., 2005. A specialized subclass of interneurons mediates dopaminergic facilitation of amygdala function. Neuron 48, 1025–1037.
Meredith, M., Westberry, J.M., 2004. Distinctive responses in the medial amygdala to same-species and different-species pheromones. J. Neurosci. 24, 5719–5725.
Minami, S., Kiyokawa, Y., Takeuchi, Y., 2019. The lateral intercalated cell mass of the amygdala is activated during social buffering of conditioned fear responses in male rats. Behav. Brain Res. 372, 112065.

Newman, S.W., 1999. The medial extended amygdala in male reproductive behavior a node in the mammalian social behavior network. Ann. NY Acad. Sci. 877, 242–257.
Paré, D., Smith, Y., 1993. The intercalated cell masses project to the central and medial nuclei of the amygdala in cats. Neuroscience 57, 1077–1090.
Petrulis, A., 2013. Chemosignals and hormones in the neural control of mammalian sexual behavior. Front. Neuroendocrinol. 34, 255–267.
Rattay, F., Bassereh, H., Fellner, A., 2017. Impact of electrode position on the elicitation of sodium spikes in retinal bipolar cells. Sci. Rep. 7, 17590.
Root, C.M., Denny, C.A., Hen, R., Axel, R., 2014. The participation of cortical amygdala in innate, odour-driven behaviour. Nature 515, 269–273.
Samuelsen, C.L., Meredith, M., 2009. Categorization of biologically relevant chemical signals in the medial amygdala. Brain Res. 1263, 33–42.
Samuelsen, C.L., Meredith, M., 2011. Oxytocin antagonist disrupts male mouse medial amygdala response to chemical-communication signals. Neuroscience 180, 96–104.
Schmidt-Hieber, C., Bischofberger, J., 2010. Fast sodium channel gating supports localized and efficient axonal action potential initiation. J. Neurosci. 30, 10233–10242.
Sosulski, D.L., Lissitsyna Bloom, M., Cutforth, T., Axel, R., Datta, S.R., 2011. Distinct representations of olfactory information in different cortical centres. Nature 472, 213–216.
Strobel, C., Sullivan, R.K.P., Stratton, P., Sah, P., 2017. Calcium signalling in medial intercalated cell dendrites and spines. J. Physiol. 595, 5653–5669.
Thompson, J.M., Neugebauer, V., 2017. Amygdala plasticity and pain. Pain Res. Manag. 2017.
Thompson, J.A., Salcedo, E., Restrepo, D., Finger, T.E., 2012. Second-order input to the medial amygdala from olfactory sensory neurons expressing the transduction channel TRPM5. J. Comp. Neurol. 520, 1819–1830.
Wang, Y., He, Z., Zhao, C., Li, L., 2013. Medial amygdala lesions modify aggressive behavior and immediate early gene expression in oxytocin and vasopressin neurons during intermale exposure. Behav. Brain Res. 245, 42–49.
Westberry, J.M., Meredith, M., 2016. GABAergic mechanisms contributing to categorical amygdala responses to chemosensory signals. Neuroscience 331, 186–196.
Westberry, J.M., Meredith, M., 2017. Characteristic response to chemosensory signals in gabaergic cells of medial amygdala is not driven by main olfactory input. Chem. Senses 42, 13–24.
Winters, B.L., Gregoriou, G.C., Kissiwaa, S.A., Wells, O.A., Medagoda, D.I., Hermes, S.M., Burford, N.T., Alt, A., Aicher, S.A., Bagley, E.E., 2017. Endogenous opioids regulate moment-to-moment neuronal communication and excitability. Nat. Commun. 8, 14611.
Wood, R.I., Coolen, L.M., 1997. Integration of chemosensory and hormonal cues is essential for sexual behaviour in the male syrian hamster: role of the medial amygdaloid nucleus. Neuroscience 78, 1027–1035.
Yao, S., Bergan, J., Lanjuin, A., Dulac, C., 2017. Oxytocin signaling in the medial amygdala is required for sex discrimination of social cues. ELife 6, e31373.
Zald, D.H., 2003. The human amygdala and the emotional evaluation of sensory stimuli. Brain Res. Rev. 41, 88–123.
Zikopoulos, B., Höistad, M., John, Y., Barbas, H., 2017. Posterior orbitofrontal and anterior cingulate pathways to the amygdala target inhibitory and excitatory systems with opposite functions. J. Neurosci. 37, 5051–5064.